Evolution of nickel silicide intrusions in silicon nanowires during thermal cycling

Alex Katsman,[1] Michael Beregovsky,[2] and Yuval E. Yaish[2]
[1]*Department of Materials Science & Engineering, Technion, Haifa 32000, Israel*
[2]*Department of Electrical Engineering, Technion, Haifa 32000, Israel*

(Received 11 November 2012; accepted 26 December 2012; published online 25 February 2013)

Thermally activated axial intrusion of nickel silicides into a silicon nanowire (NW) from pre-patterned Ni reservoirs is used in formation of nickel silicide/silicon contacts in SiNW field effect transistors. This intrusion consists usually of different nickel silicides which grow simultaneously during thermal annealing. Repeated annealing is often accompanied by local thickening and tapering of the NW, up to full disintegration of the silicide segment adjacent to Si. In the present work this process was investigated for SiNWs of various diameters in between 30 and 60 nm with pre-patterned Ni electrodes after a series of rapid thermal cycles including heating, holding at different temperatures of 400-440 °C for 5-15 s and cooling to room temperature. Kinetics of the nickel silicides axial growth was analyzed in the framework of diffusion model. This model is taking into account simultaneous formation of different nickel silicide phases and balance between transition of Ni atoms from the Ni reservoir to the NW surface, diffusion transport of these Ni atoms to the interfaces between different silicides and silicide/Si interface, and corresponding reactions of the nickel silicides' formation. Additional flux of atoms caused by the NW curvature gradients due to different radii of different silicide phases was taken into account. For a certain set of parameters thickening of the nickel-rich silicide intrusion and tapering of the monosilicide part of intrusion were obtained. © *2013 American Institute of Physics*. [http://dx.doi.org/10.1063/1.4792670]

INTRODUCTION

In the last decade field-effect transistors (FETs) based on NiSi/Si nanowire (NW) heterostructures in which the source-drain contacts are defined by the metallic NiSi NW regions have been widely observed.[1–8] Thermally activated axial intrusion of nickel silicides into the SiNW from pre-patterned Ni reservoirs is used in formation of nickel silicide/silicon contacts for SiNW FETs. However, the formation of a precisely controlled nanostructure remains a challenging problem in nanotechnology. The axial intrusion consists usually of different nickel silicides which grow simultaneously during thermal annealing. Linear and parabolic stages of the nickel silicidation were observed in the cases of predominant formation of NiSi,[2,8] θ-Ni_2Si,[9] and $NiSi_2$ phases.[10,11] The rate-limiting step providing the linear stage may be caused by transition of nickel atoms from the Ni source through the Ni/silicide interface[8] or by the reaction limit at the silicide/Si interface.[11] Repeated annealing is often accompanied by local thickening and tapering of the NW,[8,12] up to full disintegration of a silicide segment adjacent to the silicon.[13] Up to date, comprehensive understanding of these processes is still missing. Simultaneous growth of different silicides in SiNWs during rapid thermal annealing (RTA) was recently analyzed in the framework of diffusion model, which takes into account the balance between transition of Ni atoms from the Ni reservoir to the NW surface, diffusion transport of these Ni atoms from the contact area to the interfaces between different silicide phases and nickel silicide/Si interface, and corresponding reactions of Ni atoms with Si and the nickel silicides formed.[14] In the present work diffusion growth and possible instability of two-phase nickel silicide intrusions in SiNWs are investigated after a series of rapid thermal cycles including heating to annealing temperature of 400-440 °C, holding at this temperature for 5-15 s and cooling to room temperature.

The results were analyzed in the framework of diffusion model which was developed. This model includes the fluxes of Ni and Si atoms along the nickel silicides formed as well as the reactions at Si/silicide and silicide/silicide interfaces. Thickening and tapering of the silicide intrusion are explained by the presence of opposite atomic fluxes caused by curvature gradients. The latters are connected with the presence of two or more different nickel silicide phases along the intrusion segment. Quantitative agreement between experiments and theory was obtained and discussed.

EXPERIMENTAL DETAILS

The SiNWs were synthesized by the vapor-liquid-solid growth technique in an ultrahigh vacuum chemical vapor deposition chamber, with silane as the silicon precursor and gold as the catalyst.[15–17] The nanowires grown at 420 °C or 450 °C consisted of three populations. The thick (more than 60 nm in diameter) nanowires were grown in ⟨111⟩ direction, the thinner ones—in ⟨112⟩ and the thinnest—in ⟨110⟩ direction. Typical diameters of NWs grown in the ⟨112⟩ and ⟨110⟩ directions were 35–60 nm and 25–40 nm, respectively. SiNWs were oxidized at 700 °C by Chemical Vapor Deposition (CVD) reactor in oxygen flow with rate of 200 sccm and pressure of 1 atm. SiNWs were randomly dispensed from an ethanol suspension onto Si_3N_4/Si substrate and e-beam lithography was executed to pattern the metal source/drain contacts.

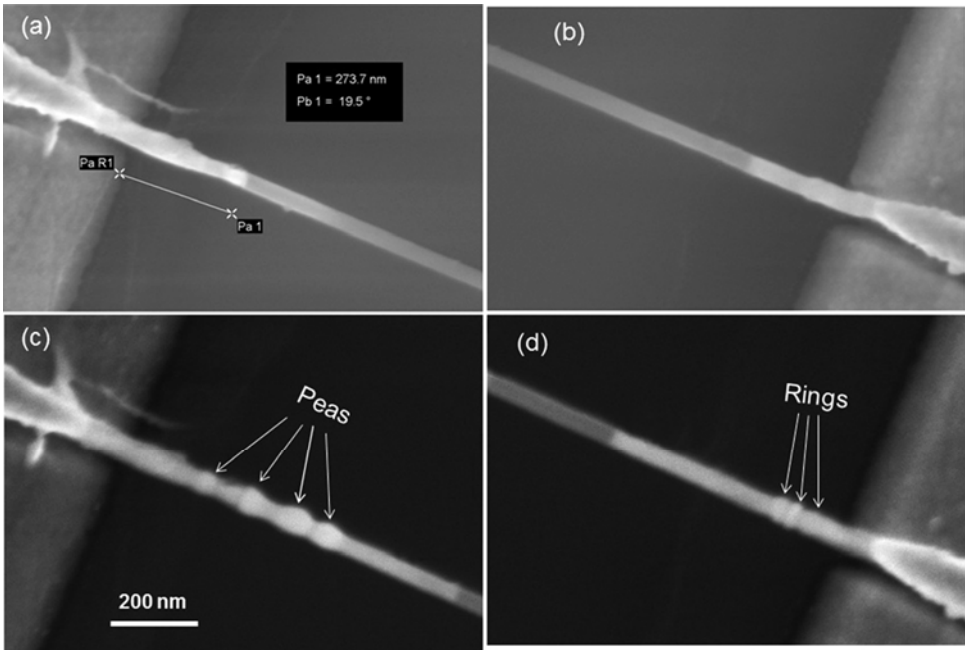

FIG. 1. (a) and (b): HRSEM images of a 28 nm-thick Ni/SiNW structure from the left (a) and right (b) sides after two subsequent thermal cycles each with annealing temperature of 420 °C for 15 s; (c) and (d): the same structures after three additional thermal cycles at 440 °C for 5 s.

Metallic Ni/Au electrodes for the source/drain contacts were deposited by e-beam evaporation. Before metal deposition, a 10 s etch in 6:1 (NH_4F:HF) buffered oxide etch (BOE) was used to remove the thermal or native oxide on the SiNWs surface in the contact area region. Careful but gentle drying of the sample was performed by nitrogen flow. It should be noted that the sample was loaded into the e-beam evaporation system within 5 min from the BOE step. Metallic electrodes were deposited by evaporation with base pressure of $2 \cdot 10^{-7}$ Torr. Excess metal was removed by a standard lift-off technique immediately after the wafer was removed from the vacuum chamber. The prepared SiNW/Ni/Au specimen had 140 nm-thick Ni layer capped with 20 nm Au. It was verified with control samples that the thin gold film on top of thick nickel layer does not affect the nickel silicide growth process.

In order to form the nickel silicide/silicon contacts, a few subsequent anneals of the sample, at 400 °C for 15 s, 420 °C for 15 s, and 440 °C for 5 s, were performed by a RTA machine with ramp rate of 1 °C/s in a nitrogen atmosphere.

After every annealing process, the silicide intrusions were investigated by high resolution scanning electron microscopy (HRSEM) and atomic force microscopy (AFM).

EXPERIMENTAL RESULTS

The axial nickel silicide intrusions formed during subsequent thermal cycles with annealing temperatures of 400°, 420°, and 440 °C are consisted from different nickel silicide phases grown simultaneously (Figs. 1–4). Morphological peculiarities of the silicide intrusions were observed as alternate thickening and tapering of the NW segments. Surprisingly, the number of thicker and thinner parts is corresponded to the number of thermal cycles included heating and cooling up to room temperature. Tapering of the silicide segments close to the Si part of the NW (apparently, monosilicide parts) was accompanied by thickening of the adjacent Ni-rich

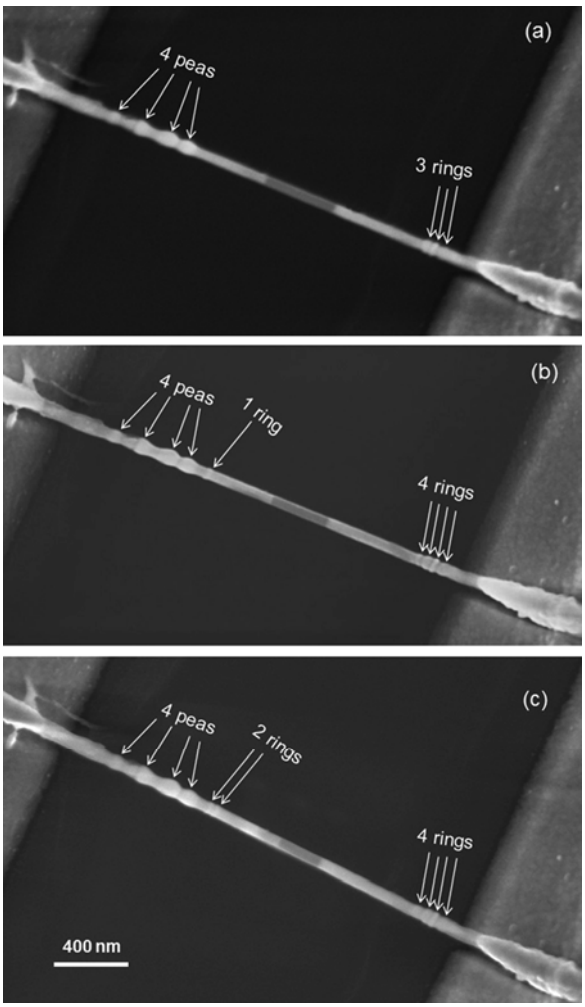

FIG. 2. (a) HRSEM images of a 28 nm-thick Ni/SiNW structure after five subsequent thermal cycles with annealing temperatures of 420 °C for 15 s (two first) and 440 °C for 5 s (three last); (b) the same structure after the 6th annealing cycle at 400 °C for 15 s; (c) the same structure after the 7th annealing cycle at 400 °C for 15 s.

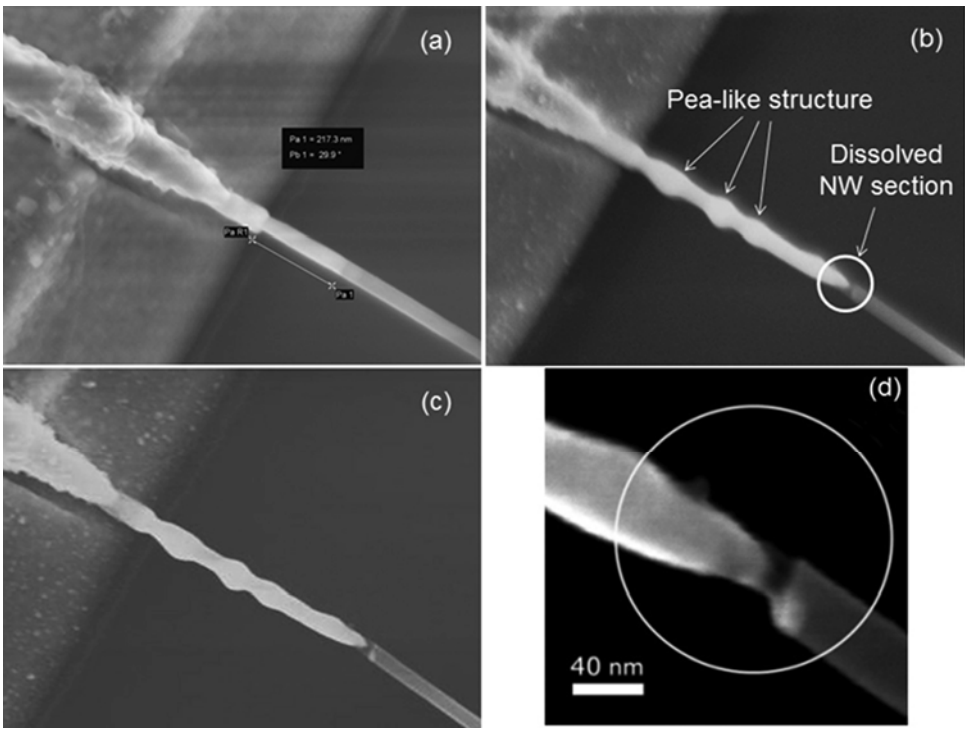

FIG. 3. (a) HRSEM images of the a 42 nm-thick Ni/SiNW structure after two subsequent thermal cycles each with annealing temperature of 420 °C for 15 s; (b) the same structure after three additional thermal cycles each at 440 °C for 5 s; (c) the same structure after the 6th thermal cycle at 400 °C for 15 s; (d) magnification of the dissolved NW section in (b).

($Ni_{1+x}Si$, $x>0$) segments as seen in Figures 1–4. In some instances the NW tapering continued up to full dissolution/disintegration of the silicide segment adjacent to the Si NW (Figures 3(b), 3(c), 4(a), 4(b), and 5). The thicker parts may have the shape of sequential rings or peas at different sides of the same NW (Figures 1, 2, and 4). Temporal evolution of the morphological peculiarities in the NiSi/Si NW is exemplified in Figures 1 and 2. In this case, the first two thermal cycles with annealing temperature of 420 °C for 15 s caused formation of a two-phase nickel silicide intrusions from both sides of the NW (Figures 1(a) and 1(b)), where the thicker part was a Ni-rich silicide and the thinner one was a monosilicide as it has been identified previously.[8,10] The further three subsequent thermal cycles each with annealing temperature of 440 °C for 5 s resulted in formation of pea-like structure at the left side and rings at the right side (Figures 1(c) and 1(d)).

The number of peas (4) and rings (3) corresponds to the number of thermal cycles. In order to understand the influence of the heating and cooling process, two additional cycles with heating to 400 °C, holding at 400 °C for 15 s and cooling to room temperature were applied. As a result, additional rings were formed on both sides of the silicide intrusion after every thermal cycle (Figures 2(b) and 2(c)). An example of full dissolution of a silicide segment after series of five thermal cycles is presented in Figure 3. In this case of full dissolution of the thinner silicide segment at the left side of the intrusion (as shown in Figures 3(b), 3(c), 4(a), and 4(c)), an additional ring after the 6th annealing cycle did not form at the left side, but still formed at the right side of the intrusion. It is interesting to note that in the case of full dissolution of the silicide segment, the NW integrity is apparently kept here by a 5 nm-thick thermal oxide shell (Figure 3(d)).

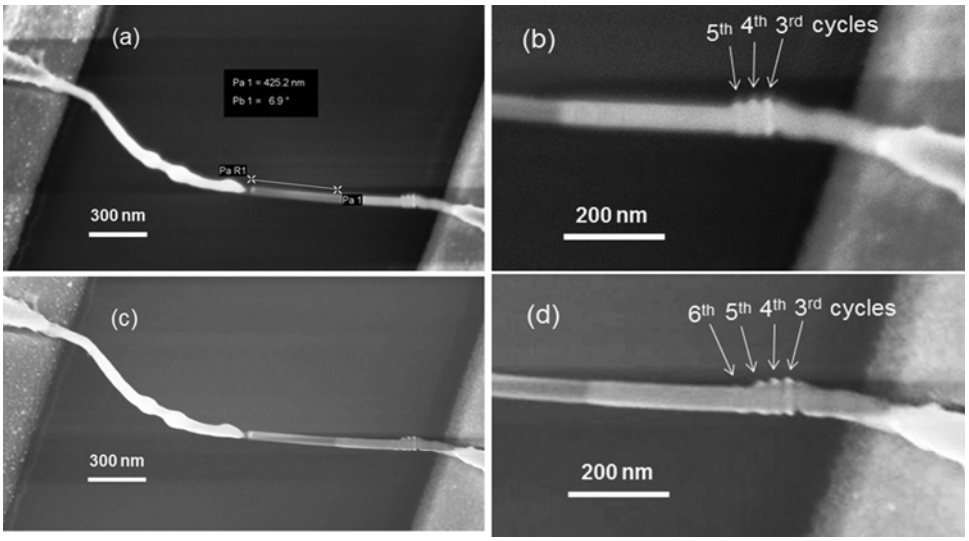

FIG. 4. (a) HRSEM images of the a 46 nm-thick Ni/SiNW structure after five subsequent thermal cycles with annealing temperatures of 420 °C for 15 s (two first) and 440 °C for 5 s (three last); (b) magnification of the right side of the structure shown in (a); (c) the same structure after the 6th thermal cycle with annealing temperature of 400 °C for 15 s; (d) magnification of the right side of the structure shown in (c).

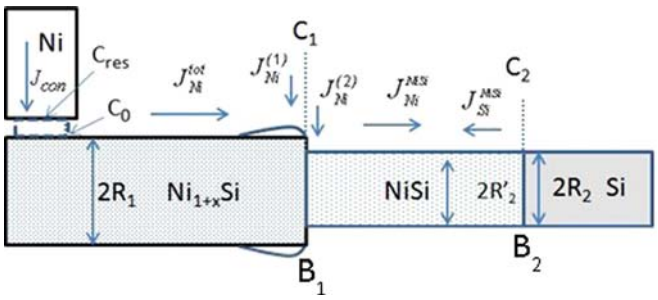

FIG. 5. Schematic diagram of evolution of nickel silicide intrusions during RTA.

DISCUSSION

Simultaneous growth of mono- and nickel-rich silicides can be described in the framework of diffusion model, which takes into account the balance between transition of Ni atoms from the Ni reservoir to the NW surface, diffusion transport from the contact area to the interfaces between different silicides and nickel silicide/Si interface, and corresponding reactions of Ni atoms with Si and the nickel silicides formed.[14] However, thickening and thinning of different parts of the nickel silicide intrusion, up to full dissolution of some part of the intrusion, cannot occur without some diffusion of silicon atoms. The Si atoms diffuse along the NiSi surface, reach the boundary NiSi/$Ni_{1+x}Si$ ($x>0$) and react there with the Ni atoms arriving this boundary from the Ni source to form a new portion of $Ni_{1+x}Si$ phase (Fig. 5). Without lose of generality, we use $x=1$ in the following discussion.

The total nickel flux, J_{Ni}^{tot}, arriving the Ni_2Si/NiSi boundary (B_1) can be divided into three parts

$$J_{Ni}^{tot} = J_{Ni}^{NiSi} + J_{Ni}^{(1)} + J_{Ni}^{(2)}, \tag{1}$$

where $J_{Ni}^{(1)}$ and $J_{Ni}^{(2)}$ are the fluxes of Ni atoms reacting with Si atoms arriving this boundary and with NiSi phase, respectively. J_{Ni}^{NiSi} is the Ni flux that reaches the NiSi/Si boundary (B_2). The corresponding reactions at boundary B_1 can be written as follows:

$$2Ni + Si \rightarrow Ni_2Si, \tag{2}$$

$$Ni + NiSi \rightarrow Ni_2Si. \tag{3}$$

Assuming $J_{Si}^{NiSi} = \theta J_{Ni}^{NiSi}$ and $J_{Ni}^{(1)} = 2J_{Si}^{NiSi}$, Eq. (1) can be rewritten

$$J_{Ni}^{tot} = J_{Ni}^{NiSi}(1+2\theta) + J_{Ni}^{(2)}. \tag{4}$$

In a steady state condition, diffusion fluxes of Ni atoms are the following:

$$J_{Ni}^{tot} = -\mathcal{L}_1 \frac{\mu_0 - \mu_1}{L_1} s_1 \approx -D_1 \frac{C_0 - C_1}{\Omega L_1} s_1, \tag{5}$$

$$J_{Ni}^{NiSi} = -\mathcal{L}_2 \frac{\mu_1 - \mu_2}{L_2} s_2 \approx -D_2 \frac{C_1 - C_2}{\Omega L_2} s_2, \tag{6}$$

where $\mathcal{L}_1$ *and* $\mathcal{L}_2$ are the kinetic coefficients (D_1 and D_2 are corresponding diffusion coefficients) along the Ni_2Si and NiSi segments of intrusion, L_1 and L2 are the lengths of Ni_2Si and NiSi segments, μ_0, μ_1, and μ_2 (C_0, C_1, and C_2) are the Ni chemical potentials (concentrations) near the Ni source, at the Ni_2Si/NiSi boundary (B_1), and at the NiSi/Si boundary (B_2), respectively. $s_1 = 2\pi R_1 \delta$, and $s_2 = 2\pi R_2 \delta$, where δ is the diffusion surface layer thickness and Ω is the atomic volume in the surface layer. The reaction flux $J_{Ni}^{(2)}$ can be written by analogy to the fluxes (5) and (6)

$$J_{Ni}^{(2)} = -\mathcal{L}_{reac} \frac{\mu_1 - \mu_{reac}}{R_1} s_{reac} \approx -D_{reac} \frac{C_1 - C_{reac}}{\Omega R_1} s_{reac}, \tag{7}$$

where $\mathcal{L}_{reac}$ is the kinetic coefficient of reaction (3) and μ_{reac} is the chemical potential of Ni atoms at the NiSi/Ni_2Si interface after reaction (B_1).

Fluxes of atoms are influenced by the surface curvature gradient, as well. The radius of the Ni_2Si segment is larger than the radius of the NiSi segment due to different number of atoms per unit length. Neglecting the difference of Si atoms per unit length, one can obtain: $R_1 = R_2(3\nu_{Ni_2Si}/2\nu_{NiSi})^{1/2}$, where ν_{Ni2Si}, and ν_{NiSi} are the atomic volumes for these two nickel-silicide phases. Using the values of $\nu_{Ni2Si} = 0.011$ nm^3 and $\nu_{NiSi} = 0.0122$ nm^3 yields the ratio $R_1/R_2 = 1.165$. The difference in cylinder radii of the Ni_2Si and NiSi phases leads to different curvatures of their surfaces.

In order to understand the influence of curvature gradient on the total flux of atoms, let us analyze the mass balance conditions at the Ni/nickel silicide contact and at the NiSi/Ni_2Si interface (B_1). The flux of Ni atoms from the reservoir through the contact layer of thickness h and area S_{con} is equal to J_{Ni}^{tot} Ref. 8

$$J_{Ni}^{tot} = J_{con} = -\mathcal{L}_{tr} \frac{\mu_{res} - \mu_0}{h} s_{con} \approx -D_{tr} \frac{C_{res} - C_0}{\Omega h} s_{con}, \tag{8}$$

where $\mathcal{L}_{tr}$ is the kinetic coefficient for transition of Ni from the reservoir to the silicide surface and μ_{res} is the chemical potential of Ni atoms in the Ni reservoir.

Using Eqs. (4)–(8) one can find the values of μ_0 and μ_1 as functions of μ_{res}, μ_{reac}, μ_2 and of dimensionless intrusion lengths $l_1 = L_1/R_1$ and $l_2 = L_2/R_1$. When the fluxes of nickel, described by Eqs. (5), and (6), are directed from the Ni reservoir to the silicon part of the NW ("positive" direction), the silicide intrusions, l_1 and l_2, grow with different kinetics, from linear to parabolic, depending on kinetic, geometric and contact parameters.[14] The sign of the flux J_{Ni}^{NiSi} (Eq. (6)) is determined by the difference of the chemical potentials

$$\mu_1 - \mu_2 = \frac{f_0(\mu_{res} - \mu_2) + (q_0 + l_1)p_0(\mu_{reac} - \mu_2)}{f_0 + (q_0 + l_1)(p_0 + 1/l_2)}, \tag{9}$$

where $f_0 \equiv [\mathcal{L}_1 s_1/\mathcal{L}_2 s_2(1+2\theta)]$, $q_0 \equiv (\mathcal{L}_1 s_1 h/\mathcal{L}_{tr} s_{con} R_1)$, and $p_0 \equiv (\mathcal{L}_{reac} s_{reac}/\mathcal{L}_2 s_2)$. As stated before, the chemical potentials μ_{res}, μ_{reac}, and μ_2 depend on the surface curvature[18]

$$\mu_{res} = \mu_{res0} + \gamma\Omega/R_1, \quad \mu_{reac} = \mu_{reac0} + \gamma\Omega/R_1, \quad \mu_2 = \mu_{20} + \gamma\Omega/R_2, \tag{10}$$

where γ is the surface energy. If $\mu_{reac} < \mu_2$ (can be possible due to the curvature term), the difference (μ_1 -μ_2) decreases

with increasing of the nickel-rich silicide length, l_1, and reaches zero at a critical value

$$l_1^{crit} = \left(\frac{f_0}{p_0}\right)\frac{\mu_{res0} - \mu_{20} - \gamma\Omega\Delta R/R_1R_2}{\mu_{20} - \mu_{reac0} + \gamma\Omega\Delta R/R_1R_2} - q_0, \qquad (11)$$

where $\Delta R = R_1 - R_2$. For values $l_1 > l_1^{crit}$, the flux J_{Ni}^{NiSi} reverses its direction, and the nickel atoms are transferred from the NiSi to the Ni-rich part of intrusion. The critical value l_1^{crit} can be estimated assuming $f_0 = 1$, $\mu_{res0} - \mu_{20} \approx k_BT \gg \gamma\Omega\Delta R/R_1R_2$ and $|\mu_{20} - \mu_{reac}| \ll \gamma\Omega\Delta R/R_1R_2$, and using typical values of $\gamma = 2\,\mathrm{J/m^2}$, $\Omega = 1.2 \cdot 10^{-29}$ $\mathrm{m^3}$, $k_BT = 9.29 \cdot 10^{-21} J$ (T =?), $R_1 = 12\,\mathrm{nm}$, and $R_2 = 10\,\mathrm{nm}$

$$l_1^{crit} \approx k_BTR_1R_2/p_0\gamma\Omega\Delta R - q_0 \simeq 30/p_0 - q_0. \qquad (11a)$$

This length can vary over a wide range of values depending on parameters of reaction (3) (incorporated in parameter p_0), on supply of Ni atoms from the reservoir (parameter q_0), and on annealing temperature influencing kinetic parameters $\mathcal{L}_i$ as well. For example, for $p_0 = q_0 = 1$, $l_1^{crit} = 29$. It should be noted that the flux J_{Ni}^{tot} does not change its direction since the difference of chemical potentials, $\mu_0 - \mu_1$, remains positive for all values of l_1. It worth to mention that since l_1^{crit} depends on temperature, it could be that during annealing cycle, $l_1^{crit} - l_1$ changes sign and the flow of Ni within the NiSi segment will change direction as well. A consequence of such behavior will discuss shortly.

Tapering and dissolution of NiSi part of intrusion

When the flux of Ni atoms along the NiSi part of intrusion reaches zero and then reverses its direction, the net flux of atoms becomes negative, since the flux of Si atoms is always directed from the Si towards the nickel reservoir. Moreover, the fluxes cannot be longer constant along the NiSi intrusion. At the Si/NiSi interface (B_2) the flux of Ni atoms should be equal to zero (there is no a source of Ni atoms there). Maximum atomic flux from the NiSi to the Ni_2Si will be realized at the NiSi/Ni_2Si interface (B_1) where the gradient curvature is maximal. For $l_1 \geq l_1^{crit}$ the difference of the chemical potentials, according to Eq. (9), can be approximated as follows:

$$\mu_1 - \mu_2 = \frac{\Delta l_1 p_0(\mu_{reac} - \mu_2)}{f_0 + (q_0 + l_1)(p_0 + 1/l_2)} \approx -\frac{\Delta l_1}{l_1}\frac{\gamma\Omega\Delta R}{R_1R_2}, \qquad (12)$$

where $\Delta l_1 = l_1 - l_1^{crit}$. The corresponding Ni flux at the NiSi/Ni_2Si interface, Eq. (6), is directed from the NiSi to the Ni_2Si and determines the rate of dissolution of the NiSi part of intrusion. It should be emphasized that dissolution of NiSi phase requires both Ni and Si fluxes being equal in their value and direction. Then, the total atomic flux along the NiSi intrusion, $J_{tot}^{NiSi} = 2J_{Ni}^{NiSi}$. Assuming a linear increase of J_{tot}^{NiSi} from zero to $2J_{Ni}^{m}$, the rate of dissolution can be written as

$$\frac{dR_2}{dt} = \Omega\delta\frac{\partial J_{tot}^{NiSi}}{\partial x} = \Omega\delta\frac{2J_{Ni}^{m}}{L_2} = -D_2C_1\frac{\Delta l_1}{l_1 l_2}\frac{\gamma\Omega\delta(R_1 - R_2)}{k_BTR_1^3R_2}. \qquad (13)$$

Furthermore, let R_1 and l_2 be constant, and $l_1 = l_1^{crit} + \alpha t^{1/2}$, where $\alpha = (4D_1\delta/R_1^3)^{1/2}$,[8] then integration of Eq. (13) results in the following equation:

$$R_1\ln\frac{R_1 - R_2}{R_1 - R_2^0} - R_2^0 + R_2 = B\left[t - \frac{2l_{crit}t^{1/2}}{\alpha} + \frac{2l_{crit}^2}{\alpha^2}\ln\left(1 + \frac{\alpha t^{1/2}}{l_{crit}}\right)\right], \qquad (14)$$

where $B = D_2C_1\gamma\Omega\delta/(k_BTR_1^3l_2)$. The time of full dissolution (until $R_2 = 0$) can be found from Eq. (14). For the case where $\alpha t^{1/2} \ll l_1^{crit}$ it can be estimated by the expression

$$t_{dis} \approx \left[\frac{3l_{crit}}{2\alpha B}\left(R_1\ln\frac{R_1}{R_1 - R_2^0} - R_2^0\right)\right]^{2/3}. \qquad (15)$$

For $D_1 = D_2 = 2 \cdot 10^{-14}\,\mathrm{m^2s^{-1}}$, $R_1 = 15\,\mathrm{nm}$, $R_2^0 = 13\,\mathrm{nm}$, $\delta = 0.5\,\mathrm{nm}$, $\alpha = (4D_1\delta/R_1^3)^{1/2} = 5.4\,\mathrm{s^{-1/2}}$, $l_{crit} = 30$, $C_1 = 0.67$, $\gamma\Omega/k_BT = 2\,\mathrm{nm}$, and $l_2 = 10$ one can obtain $B \approx 1.0$ nm/s and $t_{dis} \approx 70\,\mathrm{s}$. Interestingly, typical annealing periods in which full dissolutions were observed, last between 50 and 100 s, in good agreement with this theoretical estimation.

Local thickening: Formation of rings and pea-like bulges

Periodic thickening and thinning of the nickel silicide intrusion (Figures 1–4) is apparently connected with thermal cycling. The number of such peculiarities corresponds to the number of thermal cycles applied during RTA. As it was found, first annealing cycle resulted in formation of two-phase silicide intrusion consisted of two segments with different radii (Figures 1(a), 1(b), and 3(a)). Following annealing at comparatively low temperatures (during heating and cooling in the temperature range of 350-400 °C) may cause evolution of the intrusion in the Ni_2Si/NiSi boundary region: the critical length, l_1^{crit}, decreases with decreasing temperature (mainly, due to the increase of $p_0 \sim \mathcal{L}_{reac}/\mathcal{L}_2$, Eq. (11)), thus, while cooling the NW it is possible to enter the opposite regime where $l_1 \geq l_1^{crit}$. In this regime, according to Eq. (9), the Ni flux along the NiSi phase reverses its direction, and provides dissolution of the NiSi phase and thinning of its segment adjacent to the Ni_2Si and thickening of the latter. The result of such process can be seen, for example, in Figure 3(a). Next annealing cycle provides additional supply of nickel atoms from the Ni reservoir which causes transformation of NiSi to Ni-rich silicide again. One can assume that this process does not occur in the thinner part of the NiSi segment (where chemical potential of atoms is higher due to smaller NW radius), but immediately after this segment. By this way, new Ni_2Si segment appears in the form of a new ring (if the flux of Ni atoms is not very strong) or in the form of a pea-like bulge. This assumption is confirmed by the fact that the rings appeared during annealing at 440 °C for 5 s, were formed at the NW sides with slower intrusion growth rate, while the pea-like bulges formed at the NW sides with faster growth rate (Figures 1(c), 1(d), 2(a), 4(a), and 4(b)). When the annealing temperature was lowered to 400 °C (6th

and 7th cycles), the new rings were formed during each cycle on both sides of the intrusion (Figures 2(b) and 2(c)). In the case of full disintegration of the NiSi segment after 5 thermal cycles (Figures 3(b) and 4(a)), the 6th cycle, with annealing at 400 °C, did not cause any changes in the left side of the intrusion (Figures 3(c) and 4(c)), however, at the same time, a new ring formed on the right side of the intrusion (Figures 4(b) and 4(d)). Such behavior is apparently connected with the absence of the nickel flux from the left side after the disintegration of the NW.

Local thickening can be also resulted from additional growth of Ni_2Si phase during reaction (2). The Si atoms arriving at the $Ni_2Si/NiSi$ boundary (B_1) with the flux $J_{Si}^{NiSi} = \theta J_{Ni}^{NiSi}$ react with the part of Ni atoms ($J_{Ni}^{(1)} = 2J_{Si}^{NiSi} = 2\theta J_{Ni}^{NiSi}$) and form additional amount of Ni-rich phase. This additional phase can be evenly distributed over the surface of Ni_2Si cylinder. However, when the Ni-rich intrusion length, l_1, exceeds a critical value, l_1^{crit}, the fluxes of Ni, J_{Ni}^{tot}, and J_{Ni}^{NiSi}, have opposite directions near the $Ni_2Si/NiSi$ boundary. This may lead to accumulation of material there and formation of additional Ni-rich phase overhead the Ni_2Si cylinder in the immediate vicinity of the $Ni_2Si/NiSi$ boundary. The additional phase leads to increase of Ni-rich cylinder radius (and corresponding decrease of local curvature) resulting in accelerating dissolution of the NiSi phase. At the same time, additional curvature may appear due to formation of torus-like surface.

Let us evaluate possible increase of Ni_2Si cylinder radius due to reaction (2). The volume of additional Ni_2Si phase is giving by

$$\Delta V = 3J_{Ni}^{(1)} \cdot \nu_{Ni_2Si}\Delta t = 6\theta J_{Ni}^{NiSi} \cdot \nu_{Ni_2Si}\Delta t = 6\theta \cdot \frac{\nu_{Ni_2Si}}{\Omega}\Delta t D_2 \frac{C_1 - C_2}{L_2} 2\pi R_2 \delta. \quad (16)$$

This volume change is equal to $\Delta V = \pi(\tilde{R}_1^2 - R_1^2)\cdot h \approx 2\pi R_1 \Delta R \cdot h$, where h is the width of the additional Ni_2Si phase, and

$$\frac{\Delta R}{\Delta t} = \frac{\Delta V}{2\pi R_1 h} = \frac{6\theta \cdot \delta \cdot R_2}{h \cdot R_1}\frac{\nu_{Ni_2Si}}{\Omega} D_2 \frac{C_1 - C_2}{L_2}. \quad (17)$$

Assuming $(D_2\Delta t)^{1/2} \approx L_2 = 100\,\text{nm}$, $\delta = 0.5\,\text{nm}$, $R_1 = 18\,\text{nm}$, $R_2 = 15\,\text{nm}$, $h = 20\,\text{nm}$, $\nu_{Ni_2Si} = \Omega$, $C_1\text{-}C_2 = 0.17$, and $\theta = 0.24$, one can obtain $\Delta R = 5\,\text{nm}$. Such local thickening of the nickel-rich silicide cylinder was often observed after applying complete thermal cycling.

CONCLUSION

Evolution of nickel silicide intrusions in the NiSi/Si NWs was investigated after a series of rapid thermal cycles which included heating, holding at different temperatures of 400-440 °C for 5-15 s and cooling to room temperature. Simultaneous formation of different nickel silicide phases during RTA was confirmed. Thermal cycling resulted in sequential thickening of nickel-rich part with formation of rings or pea-like bulges at different sides of the same NW. It was accompanied by tapering of the monosilicide part up to its full dissolution and breaking of the NW. The NW curvature gradients appearing due to different radii of different silicides may play substantial role in tapering and dissolution of monosilicide segment of intrusion. Simultaneous growth of mono- and nickel-rich silicides was described for different kinetic and geometrical parameters of the system in the framework of diffusion model developed. For a certain set of parameters formation of the pea-like profile on the nickel-rich silicide surface, tapering and dissolution of the monosilicide part of intrusion were obtained.

[1]M. Weber, L. Geelhaar, A. P. Graham, E. Unger, G. S. Duesberg, M. Liebau, W. Pamler, C. Cheze, H. Riechert, P. Lugli, and F. Kreupl, Nano Lett. **6**, 2660 (2006).
[2]K.-C. Lu, W.-W. Wu, H.-W. Wu, C. M. Tanner, J. P. Chang, L. J. Chen, and K. N. Tu, Nano Lett. **7**, 2389 (2007).
[3]Y. Hu, J. Xiang, G. Liang, H. Yan, and C. M. Lieber, Nano Lett. **8**, 925 (2008).
[4]Y. Wu, J. Xiang, C. Yang, W. Lu, and C. M. Lieber, Nature **430**, 61 (2004).
[5]N. S. Dellas, B. Z. Liu, S. M. Eichfeld, C. M. Eichfeld, T. S. Mayer, and S. E. Mohney, J. Appl. Phys. **105**, 094309 (2009).
[6]W. Weber, L. Geelhaar, E. Unger, C. Cheze, F. Kreupl, H. Riechert, and P. Lugli, Phys. Status Solidi A **244**, 4170 (2007).
[7]K. Sarpatwari, N. S. Dellas, O. O. Awadelkarim, and S. E. Mohney, Solid-State Electron. **54**, 689 (2010).
[8]Y. E. Yaish, A. Katsman, G. M. Cohen, and M. Beregovsky, J. Appl. Phys. **109**, 094303 (2011).
[9]N. S. Dellas, M. Abraham, S. Minassian, C. Kendrick, and S. E. Mohney, J. Mater. Res. **26**, 2282 (2011).
[10]K. Ogata, E. Sutter, X. Zhu, and S. Hofmann, Nanotechnology **22**, 365305 (2011).
[11]Y. Chen, Y. C. Lin, C. W. Huang, C. W. Wang, L. J. Chen, W. W. Wu, and Y. Huang, Nano Lett. **12**, 3115 (2012).
[12]Y.-C. Lin, Y. Chen, D. Xu, and Y. Huang, Nano Lett. **10**(11), 4721 (2010).
[13]A. Katsman, M. Beregovsky, and Yu. E. Yaish, "Diffusion Instability and Tapering of Nickel Silicide Intrusions in Silicon Nanowires," MRS Proceedings, 1408, mrsf11-1408-bb10-31, 2012, doi:10.1557/opl.2012.93.
[14]A. Katsman, Y. Yaish, and M. Beregovsky, Defect Diffus. Forum **323–325**, 427 (2012).
[15]R. S. Wagner and W. C. Ellis, Appl. Phys. Lett. **4**, 89 (1964).
[16]J. Westwater, D. P. Gosain, S. Tomiya, S. Usui, and H. Ruda, J. Vac. Sci. Technol. B **15**, 554 (1997).
[17]A. M. Morales and C. M. Lieber, Science **279**, 208 (1998).
[18]W. W. Mullins, J. Appl. Phys. **30**, 77–83 (1959).